the four-noded knot has roughly tetrahedral symmetry, and it is possible to create star-shaped arrangements where the central four-noded knot coordinates to four other knots. □

1. Katrich, V. et al. Geometry and physics of knots. Nature 384, 142–145 (1996).
2. Stasiak, A., Katrich, V., Bednar, J., Michoud, D. & Dubochet, J. Electrophoretic mobility of DNA knots. Nature 384, 122 (1996).
3. Rolfsen, D. Knots and Links (Publish or Perish, Berkeley, CA, 1976).
4. Fuller, F. B. The writhing number of a space curve. Proc. Natl Acad. Sci. USA 68, 815–819 (1971).
5. Fuller, F. B. Decomposition of the linking number of a closed ribbon: a problem from molecular biology. Proc. Natl Acad. Sci. USA 75, 3557–3561 (1978).
6. Janse van Rensburg, E. J., Orlandini, E., Sumners, D. W., Tesi, M. C. & Whittington, S. G. The writhe of knots in the cubic lattice. J. Knot Theory Ramif. 6, 31–44 (1997).
7. Calugareanu, G. L'intégral de Gauss et l'analyse des noeuds tridimensionnels. Rev. Math. Pur. Appl. 4, 5–20 (1959).
8. Vologodskii, A. V., Levene, S. D., Klenin, K. V., Frank-Kamenetskii, M. & Cozzarelli, N. R. Conformational and thermodynamic properties of supercoiled DNA. J. Mol. Biol. 227, 1224–1243 (1992).
9. Pieranski, P. Search of ideal knots. ProDialog 5, 111–120 (1996).

The dynamics of partially extended single molecules of DNA

Stephen R. Quake*, **Hazen Babcock & Steven Chu**

Physics Department, Stanford University, Stanford, California 94305, USA

The behaviour of an isolated polymer floating in a solvent forms the basis of our understanding of polymer dynamics[1,2]. Classical theories describe the motion of a polymer with linear equations of motion, which yield a set of 'normal modes', analogous to the fundamental frequency and the harmonics of a vibrating violin string. But hydrodynamic interactions make polymer dynamics inherently nonlinear, and the linearizing approximations required for the normal-mode picture have therefore been questioned[1]. Here we test the normal-mode theory by measuring the fluctuations of single molecules of DNA held in a partially extended state with optical tweezers. We find that the motion of the DNA can be described by linearly independent normal modes, and we have experimentally determined the eigenstates of the system. Furthermore, we show that the spectrum of relaxation times obeys a power law.

The starting point for describing the motion of a polymer is the Rouse model of beads interconnected with gaussian springs. If the interactions between different segments (beads) of the polymer R_n and R_m (n and m denote the order of the beads along the length of the polymer) are localized to nearest neighbours, each of the segments R_n satisfies a linear differential equation decoupled from the other segments. This linear system allows one to describe the dynamics in terms of a set of normal modes with mode amplitudes X_p defined as $X_p = (1/N)\int_0^N R_n \cos(\pi pn/N)\mathrm{d}n$ (where p is an integer denoting the pth mode and N is the total number of beads). Associated with the normal modes is a set of relaxation times, τ_p, which describe the decay in the time correlations of the normal-mode amplitudes $\langle X_p(t)X_q(0)\rangle \sim \delta_{pq}e^{-t/\tau_p}$ (where q is the qth mode).

Hydrodynamic interactions between segments of the polymer were first included by Zimm[3] by assuming the surrounding fluid is incompressible and obeys the Navier–Stokes equation (known as the Kirkwood approximation[4]). The resulting coupling of each polymer segment R_n to all of the other segments R_m leads to a

nonlinear set of differential equations as the coupling depends on the instantaneous configuration of the polymer. These equations can be linearized by first averaging the distance $|R_m - R_m|$ between segments over the distribution of accessible configurations. This so-called 'pre-averaging' approximation linearizes the set of coupled differential equations and allows one to construct a set of normal modes similar to the Rouse modes.

It has been argued that a normal-mode description of a polymer can be only a rough approximation of the true dynamics and may not have any fundamental validity[1]. Apart from questioning the soundness of the pre-averaging approximation, other nonlinear effects such as excluded-volume effects, forbidden crossings, and knots were not included in Zimm's treatment. These and other nonlinear effects have led de Gennes[1] and others to emphasize dynamical scaling laws rather than a normal-mode description. Scaling laws link relaxation rates to the spatial scale of interest, but do not require knowledge of the precise shape of the relaxation spectrum. On the other hand, the normal-mode concept requires that the relaxation spectrum be described by a set of discrete frequencies.

The analysis of the relaxation of polymers perturbed from equilibrium can yield a frequency spectrum by taking the inverse Laplace transform of the relaxation spectrum, but these methods do not provide an unambiguous decomposition into discrete frequencies[5,6]. Dynamic light-scattering experiments[7,8], viscoelastic and oscillatory flow birefringence studies[9–12] and transient electric birefringence experiments[13,14] probe relaxation rates at size scales considerably smaller than the overall coil size, but these measurements represent an average over what could be a continuous spectrum of relaxation rates. Dielectric relaxation of dipole-inverted *cis*-polyisoprene has been used to measure the first two normal-mode eigenfunctions, and a tentative extrapolation was used to derive the third[15–17]. However, this method does not measure a relaxation mode spectrum, and does not discriminate between linear and nonlinear effects.
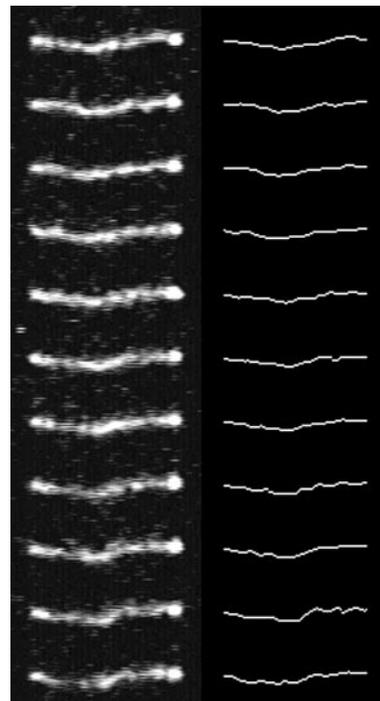
Figure 1 Video images of single molecules of DNA held at an extension of 12 µm. The column on the left shows a series of successive raw video images; the column on the right shows the corresponding parametrizations used in the data analysis.

* Present address: Department of Applied Physics, Caltech, MS 128-95, Pasadena, California 91125, USA.
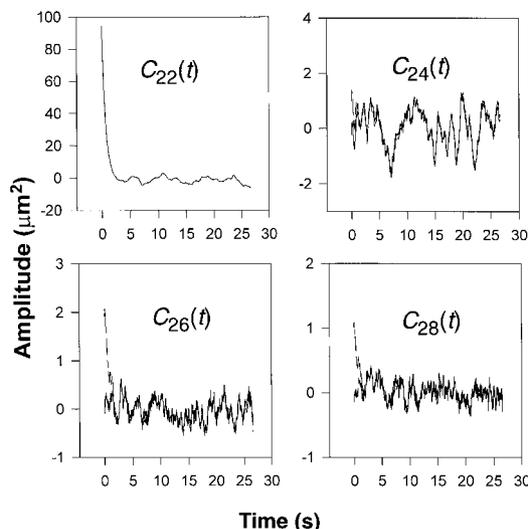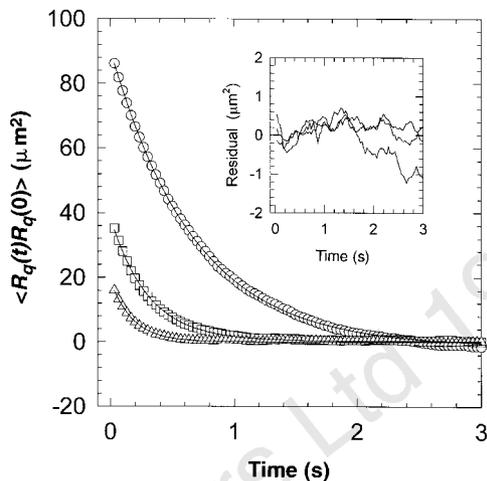
Figure 2 Comparison of the sine basis and the normal-mode basis for several matrix elements of DNA held at 10 μm extension. The correlation function $C_{pq}(t)$ represents eigenbasis correlation matrix $\langle X_p^{(y)}(t)X_q^{(y)}(0)\rangle$ for solid lines and the sine basis correlation matrix $\langle U_p^{(y)}(t)X_q^{(y)}(0)\rangle$ for dashed lines. We note that in the normal-mode basis, there are no off-diagonal elements above the level of noise fluctuations. The increasing frequency of the characteristic fluctuations for the cross-correlation of mode 2 with successively higher modes may be seen in this figure.


Figure 3 Relaxation curves and exponential fits for $q = 2$, 3, and 4 (circles, squares and triangles, respectively) at extension 10 μm. Inset, residuals from the fits, showing a small systematic deviation from pure exponential relaxation. There is a measurement error in assigning the parametrization of the polymer; this causes a systematic error in the $t = 0$ correlation matrix. If $R_n(t)$ denotes the actual position of the polymer and $\epsilon_n(t)$ denotes the measurement error, then the measured quantity is $R_n(t) + \epsilon_n(t)$. $\langle(R_q(t) + \epsilon_q(t))(R_q(0) + \epsilon_q(0))\rangle = \langle(R_q(t)R_q(0)\rangle + \langle\epsilon_q(t)\epsilon_q(0)\rangle$, where the cross terms $\langle R_q(t)\epsilon_q(0)\rangle + \langle\epsilon_q(t)R_q(0)\rangle = 2\langle R_q\rangle\langle\epsilon_q\rangle$ are zero. The measurement error should be independent of time, so $\langle\epsilon_q(t)\epsilon_q(0)\rangle$ vanishes for $t \neq 0$. We checked this by fitting the relaxation function to two exponentials; one relaxation time was always degenerately small, while the amplitudes were in agreement with our other estimations of the signal and noise. Thus, the intrinsic noise has a systematic effect on only the $t = 0$ point of the correlation function. That point was discarded before fitting the relaxation to an exponential function.

We have tested the supposition that polymer motion can be described by a set of normal modes by recording the images of partially extended 20-μm-long pieces of DNA driven by brownian motion. The DNA is suspended in solution by attaching 0.3-μm polystyrene spheres to the ends of the molecule that serve as 'handles' for two optical tweezers[18]. The DNA, fluorescently stained with the dye YOYO-1 (Molecular Probes, Eugene, OR) and illuminated by 488-nm light, was held in a partially extended state with optical tweezers while the images were recorded by video microscopy (Fig. 1). Analysis of the static properties of partially extended polymers (to be presented elsewhere) shows that intercalation by YOYO-1 increases the length of λ DNA from 16.4 to 20 μm, and increases the persistence length from 50 to 66 nm.

The optical images were converted into parametrized descriptions of the DNA location as described below. If the line joining the two beads defines the x-axis, we analyse the polymer configuration in terms of displacements $R_n^{(y)}(t)$ along the y-axis. The boundary conditions of fixed end points suggests that a good first approximation to the projection of the normal modes describing the y-motion would be the sine functions with amplitudes $U_p^{(y)} = (1/N)\int_0^N R_n^{(y)}(t)\sin(\pi pn/N)dn$. Normal modes have also been calculated for boundary conditions where only one end of the polymer is fixed[19].

After computing $U_p^{(y)}(t)$ by taking a sine transform of $R_n^{(y)}(t)$ (ref. 20), we calculated the cross-correlation matrix $\langle U_p^{(y)}(t)U_q^{(y)}(0)\rangle$ for the first eight sine modes. This matrix is not diagonal and has off-diagonal relaxations (Fig. 2). For example, for 10 μm extension the amplitude of the $\langle U_2^{(y)}(0)U_6^{(y)}(0)\rangle$ matrix element is 1.9 μm², as compared to the 86.2 μm² for the $\langle U_2^{(y)}(0)U_2^{(y)}(0)\rangle$ element and 16.0 μm² for the $\langle U_6^{(y)}(0)U_6^{(y)}(0)\rangle$ element. Random noise in the measurement can be estimated from

the r.m.s. fluctuations of the matrix elements after all correlations have disappeared. The r.m.s. fluctuations of $\langle U_2^{(y)}(t)U_6^{(y)}(0)\rangle$, $\langle U_2^{(y)}(t)U_2^{(y)}(0)\rangle$ and $\langle U_6^{(y)}(t)U_6^{(y)}(0)\rangle$ were computed between $6.7 < t < 26.7$ seconds, yielding 0.22 μm², 2.05 μm² and 0.07 μm², respectively. The off-diagonal relaxations are therefore statistically significant and show that the sine functions are not the normal modes of the system.

Zimm recognized that the sine basis is only an approximation to the exact eigenbasis, and calculated higher-order corrections[21]. Similarly, we sought an improved eigenbasis constructed for the sine basis $u_k(x, t) = U_k^{(y)}(t)\sin(k\pi x/L)$, where L is the distance between the end points of DNA, in the form $x_i^{(y)}(x, t) = \Sigma_k B_{ik}x_k^{(y)}(x, t)$. The condition for the time correlations of the normal-mode amplitudes $X_i(t)$ becomes

$$\langle X_i(t)X_j(0)\rangle = \left\langle\left(\sum_k B_{ik}U_k(t)\right)\left(\sum_l B_{jl}U_l(0)\right)\right\rangle$$

$$= \sum_{k,l} B_{ik}B_{jl}\langle U_k(t)U_l(0)\rangle$$

$$= \delta_{ij}A_i e^{-t/\tau_i}$$

We solved for the matrix B by diagonalizing the cross-correlation matrix for $t = 1/30$ s (one video frame). Figure 2 shows that the resulting basis, given in Table 1, satisfies the orthogonality condition. Time cross-correlations of different mode amplitudes were indistinguishable from noise. If normal modes did not exist, the transformation matrix would be a function of time and we would expect to see non-zero correlation functions in a time t between 1/30 s and the mean of τ_p and τ_q. In addition to demonstrating the
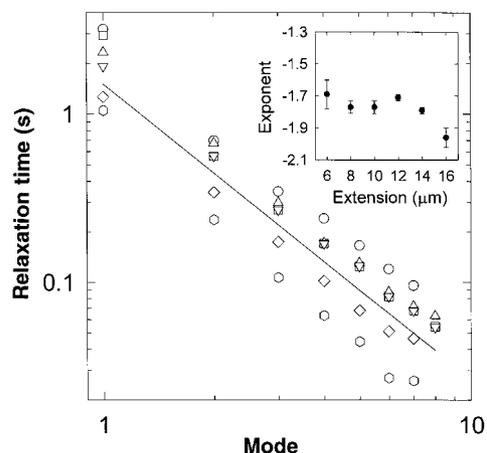
Figure 4 Relaxation time versus mode (q) from fitting to single exponentials (circle, 6 μm extension; square, 8 μm; down triangle, 10 μm; up triangle, 12 μm; diamond, 14 μm; hexagon, 16 μm). The line has a slope of −1.7. There is a dependence of relaxation time on extension: the greater the extension, the higher the 'string tension' and the faster the relaxation. The ultimate limit of how many modes we could resolve was determined by both the temporal and spatial resolution of the system. The time resolution of one video frame (= 0.033 s) limited the most extended polymers to eight modes. The spatial resolution was lowest for the least extended polymers, as the 'slack' in the DNA increases the width of the image. For the smallest extension (6 μm) the average full-width at half-maximum of the image in the transverse direction was 0.71 μm, indicating a cut-off after eight modes. Inset, fitted exponents for the mode structure as a function of extension.

Table 1 Normal-mode eigenbasis

1.000	0.000	−0.011	−0.011	−0.019	−0.004	−0.008	0.002
0.000	0.999	0.029	−0.018	−0.006	−0.024	−0.005	−0.011
0.010	−0.027	0.997	0.023	−0.043	0.002	−0.044	−0.007
0.012	0.020	−0.024	0.997	0.020	−0.025	−0.021	−0.046
0.019	0.007	0.038	−0.044	0.996	0.010	−0.073	0.000
0.005	0.024	−0.004	0.027	−0.017	0.999	0.003	−0.041
0.010	0.003	0.047	0.023	0.074	−0.001	0.995	−0.027
0.000	0.012	0.009	0.045	−0.007	0.040	0.049	0.998

Columns show the normal modes expressed in terms of a sum of sine vectors for the 10-μm extension. The rows are the mode numbers. For example, column 8 shows that the eighth normal mode has an amplitude 0.998 of $\sin(8\pi n/N)$, −0.027 of $\sin(7\pi n/N)$ and −0.041 of $\sin(6\pi n/N)$.

orthogonality of the normal modes, we show in Fig. 3 that the diagonal relaxation functions $\langle X_p^{(y)}(t)X_p^{(y)}(0)\rangle$ are well described by a single exponential decay as required for a linear dynamical system.

Figure 4 shows that the relaxation times τ_p scale as a power law over almost two decades of time. The Zimm model for a coiled polymer predicts an exponent of −1.5 for a Θ-solvent[2] and −1.8 for a good solvent. DeGennes has predicted[22] that a highly extended polymer will have an exponent of −2.0. Caution must be used in comparing the observed power-law scaling to dynamical models that were derived for conditions where the end points are not constrained. Although it is known that our buffer conditions correspond to a good solvent for DNA[23], it has been suggested that an extended polymer will behave as in an ideal solvent on moderate to long length scales such as we measured[24,25]. Also, the pre-averaged distances for a partially extended polymer are different than for a free polymer. For an unstretched chain, $\langle|R_n - R_m|\rangle \sim |n-m|^{0.5}$ for an ideal solvent and $|n-m|^{0.6}$ for a good solvent leading to relaxation times that scale as $\tau_p \approx p^{-1.5}$ or $p^{-1.8}$, respectively. For partially extended polymers, at distances $|n-m| \gg 1$, we expect $\langle|R_n - R_m|\rangle^{-1}_{\text{pre-averaged}} \approx |n-m|^{-1.0}$, but for $n \approx m$, $|n-m|^{-\alpha}$ where the exponent α might be some value between 0.5 and 1.0. Clearly, a calculation of the pre-averaged hydrodynamic tensor for our geometry will have to be done before one compares these results to a particular dynamical model. □

Methods

Sample preparation. λ-Phage DNA was attached to streptavidin-coated beads via biotinylated oligonucleotides that hybridized to the single-stranded ends of λ DNA. The λ DNA and one of the oligonucleotides were mixed in equal molar amounts in 50 mM NaCl−TE (10 mM Tris-Cl, 1 mM EDTA, pH 8.0), heated to 70 °C for 10 min, and allowed to anneal to room temperature for 2–3 h. The opposite oligonucleotide was mixed with streptavidin beads in about 2× excess to streptavidin binding sites, and allowed to incubate for 8 h before being washed three times by centrifugation. Equal molar amounts of biotinylated DNA, oligo-coated beads, and streptavidin beads were mixed and allowed to incubate for 12 h at room temperature in 50 mM NaCl−TE. The resulting bead−DNA−bead complexes were diluted by a factor of 10 into a staining solution contain TE, 2 mM NaCl, 100 nM YOYO, 1% β-mercaptoethanol, and 0.1% Tween-20. After 45–60 min of staining, the complexes were diluted by another factor of 10 into a high-viscosity TE buffer containing a final concentration of 71% (w/v) glycerol, 2 mM NaCl, and 0.1% Tween-20. To retard photobleaching of the dye, 0.1 mg ml^{-1} glucose oxidase, 0.04 mg ml^{-1} catalase, and 0.4% glucose were added.

Experimental procedure. The optical tweezers were made by focusing two independently controllable infrared (1.064-μm) Nd : YAG laser beams through a ×63, 1.4 numerical aperture microscope in a home-made microscope with a measured resolution of 0.25 μm. The DNA was held 10 μm below the surface of a 30-μm-deep cell made from a microscope slide and coverslip sealed with epoxy. The fluorescent images were recorded with an image-intensified CCD camera with a video rate of 30 Hz. Because the fundamental relaxation time of a polymer is proportional to viscosity, we increased the effective time resolution of the experiment by increasing the viscosity from 0.01 to 0.2 poise with the addition of 71% glycerol (w/v). We took data from 37 different molecules held at six different extensions ranging between 30% and 80% of the full length of the molecule. An average of 24 min (43,200 video frames) of data were taken at each extension.

Data analysis. Spatial noise in the images were filtered out by convolving each image with a gaussian of width 0.42 μm before finding the fluorescence maxima. Using continuity of the DNA, an algorithm tracked the fluorescent peak from one bead to the other and back again. As the DNA fluctuated in and out of the focal plane, parts of its image broadened and occasionally disappeared. The fitting program discarded those points; 98% of the data was retained, and a visual and manual check ensured that the fitting program was not giving skewed values. Although details of the DNA configuration below the 0.25 μm resolution of the microscope are not seen, we estimate that the centre of the image is determined with an uncertainty of ±1 pixel which is ±0.14 μm. We showed that the resulting 'pixellation' of the images does not affect the data analysis by artificially increasing the linear pixel size by a factor of two; the results of the subsequent data analysis did not change. The beads are free to rotate in the traps; this allows the ends of the polymer a small amount of motion not greater than the radius of the bead. Also, the beads absorb some of the YOYO and fluoresce brightly; this causes blooming on the video image and prevents us from locating the precise end points of the DNA. As we infer the locations of those end points from the locations of the beads, there is a small systematic overestimation of the distance of the distance of the DNA from its equilibrium position as it fluctuates above and below the imaginary line which connects the two beads. We put that extra degree of freedom of the end points into a computer simulation of a bead−spring model with the exact hydrodynamic tensor. For exponential fits, the power-law exponent of the simulated mode structure with mobile end points was 2.5% smaller than the value for fixed end points, with a 2.5% statistical error on the fit. Thus the rotation of the beads has only a small systematic effect on the data. One can correct for this effect by multiplying the measured exponents by 1.025.

1. de Gennes, P. G. *Scaling Concepts in Polymer Physics* (Cornell Univ. Press, Ithaca, NY, 1979).
2. Doi, M. & Edwards, S. *The Theory of Polymer Dynamics* (Clarendon, Oxford, 1986).
3. Zimm, B. H. Dynamics of polymer molecules in dilute solution: viscoelasticity, flow birefringence and dielectric loss. *J. Chem. Phys.* **24**, 269–278 (1956).
4. Kirkwood, J. & Riseman, J. The intrinsic viscosities and diffusion constants of flexible macromolecules in solution. *J. Chem. Phys.* **16**, 565–573 (1948).
5. Perkins, T., Quake, S., Smith, D. & Chu, S. Relaxation of a single DNA molecule observed by optical microscopy. *Science* **264**, 822–826 (1994).
6. Pecora, R. DNA—A model-compound for solution studies of macromolecules. *Science* **251**, 893–898 (1991).
7. Sorlie, S. & Pecora, R. A dynamic light-scattering study of 4 DNA restriction fragments. *Macromolecules* **23**, 487–497 (1990).
8. Adam, M. & Delsanti, M. Dynamical properties of polymer solutions in good solvent by Rayleigh scattering experiments. *Macromolecules* **10**, 1229–1237 (1977).
9. Sahouani, H. & Lodge, T. P. Onset of excluded-volume effects in chain dynamics. *Macromolecules* **25**, 5632–5642 (1992).
10. Amelar, S. *et al*. Dynamic properties of low and moderate molecular-weight polystyrenes at infinite dilution. *Macromolecules* **24**, 3505–3516 (1991).
11. Sammler, R. L. *et al*. Polydispersity effects on dilute-solution dynamic properties of linear homopolymers. *Macromolecules* **23**, 2388–2396 (1990).
12. Johnson, R., Schrag, J. & Ferry, J. Infinite-dilution viscoelastic properties of polystyrene in θ-solvents and good solvents. *Polym. J.* **1**, 742–749 (1970).
13. Hong, M. K. *et al*. Internal dynamics of DNA probed by transient electric birefringence. *Phys. Rev. Lett.* **68**, 1430–1433 (1992).
14. Lewis, R., Pecora, R. & Eden, D. Transient electric birefringence measurements of the rotational and internal bending modes in monodisperse DNA fragments. *Macromolecules* **19**, 134–139 (1986).
15. Watanabe, H., Yao, M. & Osaki, K. Comparison of dielectric and viscoelastic relaxation behavior of polyisoprene solutions—coherence in subchain motion. *Macromolecules* **29**, 97–103 (1996).
16. Watanabe, H., Yamada, H. & Urakawa, O. Dielectric-relaxation of dipole-inverted cis-polyisoprene solutions. *Macromolecules* **28**, 6443–6453 (1995).
17. Watanabe, H., Urukawa, O. & Kotaka, T. Slow dielectric-relaxation of entangled linear cis-polyisoprenes with asymmetrically inverted dipoles. 1. Bulk systems. *Macromolecules* **26**, 5073–5083 (1993).
18. Ashkin, A., Dziedzic, J., Bjorkholm, J. & Chu, S. Observation of a single-beam gradient force optical trap for dielectric particles. *Opt. Lett.* **11**, 288–290 (1986).
19. Marciano, Y. & Brochard-Wyart, F. Normal-modes of stretched polymer-chains. *Macromolecules* **28**, 985–990 (1995).
20. Press, W., Teukolsky, S., Vetterling, W. & Flannery, P. *Numerical Recipes* (Cambridge Univ. Press, New York, 1994).
21. Zimm, B., Roe, G. & Epstein, L. Solution of a characteristic value problem for the theory of chain molecules. *J. Chem. Phys.* **24**, 279–280 (1956).
22. De Gennes, P. G. Coil-stretch transition of dilute flexible polymers under ultrahigh velocity gradients. *J. Chem. Phys.* **60**, 5030–5042 (1974).
23. Smith, D., Perkins, T. & Chu, S. Dynamical scaling of DNA diffusion-coefficients. *Macromolecules* **29**, 1372–1373 (1996).
24. Pincus, P. Excluded volume effects and stretched polymer chains. *Macromolecules* **9**, 386–388 (1976).
25. Pincus, P. Dynamics of stretched polymer chains. *Macromolecules* **10**, 210–213 (1977).

Correspondence and requests for materials should be addressed to S.C. (e-mail: schu@leland.stanford.edu).

Multiple episodes of aridity in southern Africa since the last interglacial period

Stephen Stokes*†, David S. G. Thomas‡
& Richard Washington*

* School of Geography, University of Oxford, Mansfield Road,
Oxford OX1 3QJ, UK
† Research Laboratory for Archaeology and the History of Art,
University of Oxford, Mansfield Road, Oxford OX1 3TB, UK
‡ Sheffield Centre for International Drylands Research, Department of Geography,
University of Sheffield, Sheffield S10 2TN, UK

There is generally a dearth of evidence of the nature of Quaternary climate change within desert systems, which has limited previous interpretations of past environmental change at low latitudes. The Last Glacial Maximum has previously been identified as the peak of Late Quaternary aridity, when desert systems expanded to five times their present extent[1–3], and low-latitude aridity has been described for previous glaciations[4]. But little evidence has been derived directly for large desert basins, particularly southern Africa. Here we report new chronological (optical dating) evidence of arid episodes recorded in aeolian sediments from the Mega Kalahari sand sea. Episodic aeolian activity is recorded at the northeastern desert margin, whereas more sustained activity is evident from the southwestern desert core. Several significant arid events are apparent since the last interglacial period, with dune-building (arid) phases at ~95–115, 41–46, 20–26 and 9–16 kyr before present. Existing atmospheric general circulation model simulations and independent palaeoclimate data indicate that the changes in aridity are related to changes in the northeast–southwest summer rainfall gradient, which are in turn related to sea surface temperatures in the southeastern Atlantic Ocean.

The $2.5 \times 10^6 \, \text{km}^2$ Mega Kalahari is the world's most continuous area of aeolian sand sea which is dominated by variably degraded and pedogenically modified, currently inactive, linear dunes[5] (Fig. 1). The development and evolution of the extensive Kalahari linear dune systems has not until now been directly dated. Phases of aridity and dune development have previously been inferred from gaps within subcontinental humid chronologies[6,7], or by assumed mirroring of Northern Hemisphere conditions[8]. We have determined the timing of dune building and associated palaeoaridity along the present day northeast–southwest summer rainfall gradient by optically dating[9] dune sediments from geographically and morphologically wide-ranging aeolian deposits. Past changes in aeolian dynamism is assumed to be related to shifting rainfall intensities along the gradient (Fig. 1).

The effect of this northeast–southwest rainfall gradient on aeolian activity provides an opportunity to determine the sensitivity of the climate system to changing boundary conditions since the last interglacial. The climatology of this gradient is an infrequently studied element of the general circulation of the subcontinent, yet one that is accurately captured in all present-day leading general circulation models[10,11]. It originates from the Earth's largest cross-continental zonal asymmetry of tropical convection; the inter-tropical convergence zone (ITCZ) in the southwestern Indian Ocean occupies the most southerly location of any ocean at 23° S, whereas tropical convection in the eastern Atlantic Ocean is seldom found south of 5° N (ref. 11). Convection over southern Africa aligns almost meridionally over the subcontinent. Differences in the latitude of convection in the adjacent oceans relates directly to sea surface temperatures (SSTs).

The southwestern Indian Ocean is the warmest ocean at 23° S whereas the southeastern Atlantic is the coldest (present-day January mean of 27.5 and 21.6 °C, respectively). The extreme SST contrast across the subcontinent determines the southern African rainfall gradient (Fig. 1). Wetter conditions east of the Kalahari result from disturbances in the tropical easterlies associated with the Mascarene anticyclone. Westward propagation of easterly waves off the African subcontinent is blocked by cold stable air overlying the Benguela Current. Conditions west of the wave axis are therefore dry. Intense subsidence into subtropical anticyclones dominate the climatology of the austral winter, ensuring aridity. The elevated southern African land mass (2,000 m) cools through longwave emission, thereby providing an interhemispheric sink for Asian monsoon outflow. Few deserts provide a suite of controls on the rainfall regime as diverse as the Kalahari.

Although the controls on aeolian sedimentation, particularly in the case of linear dune development[12], may be complex we believe that our chronology of dune construction reflects periods of regionally enhanced aridity. In the northeastern Kalahari, mean rainfall today exceeds 400 mm yr^{-1}, and the pedogenically modified and vegetated surfaces of degraded linear dunes prohibits aeolian activity. In the southwestern Kalahari the present mean annual rainfall is 150–200 mm. Episodic, localized aeolian activity is confined to dune crests and controlled by variations in vegetation cover induced by interannual variations in rainfall and intensive grazing, but is in any case significantly restricted by present-day low